

Downstream Effects of Upstream Causes

Bradley C. Saul *

Department of Biostatistics, University of North Carolina Chapel Hill

Michael G. Hudgens

Department of Biostatistics, University of North Carolina Chapel Hill

Michael A. Mallin

Center for Marine Science, University of North Carolina Wilmington

March 20, 2018

Abstract

The United States Environmental Protection Agency considers nutrient pollution in stream ecosystems one of the U.S.' most pressing environmental challenges. But limited independent replicates, lack of experimental randomization, and space- and time-varying confounding handicap causal inference on effects of nutrient pollution. In this paper the causal g-methods are extended to allow for exposures to vary in time

*We would like to thank Dr. Rebecca Benner and the Nature Conservancy of North Carolina for compiling and providing the data. We would also like to thank all those who collected and collated these data in order to protect the Cape Fear watershed. The causal inference with interference research group at UNC (Brian Barkley, Sujatro Chakladar, and Wen Wei Loh) plus Mary Kirk Wilkinson provided helpful feedback and critical support throughout this project. We also thank the Associate Editor and two anonymous for helpful comments. This work was partially supported by NIH grant R01 AI085073 and the Lower Cape Fear River Program. The content is solely the responsibility of the authors and does not necessarily represent the official views of the National Institutes of Health.

and space in order to assess the effects of nutrient pollution on chlorophyll a – a proxy for algal production. Publicly available data from North Carolina’s Cape Fear River and a simulation study are used to show how causal effects of upstream nutrient concentrations on downstream chlorophyll a levels may be estimated from typical water quality monitoring data. Estimates obtained from the parametric g-formula, a marginal structural model, and a structural nested model indicate that chlorophyll a concentrations at Lock and Dam 1 were influenced by nitrate concentrations measured 86 to 109 km upstream, an area where four major industrial and municipal point sources discharge wastewater.

Keywords: g-formula, marginal structural models, potential outcomes, structural nested models

1 Introduction

Nutrient pollution of U.S. streams costs billions of dollars each year (Dodds et al., 2009). The EPA calls reducing nutrient pollution in U.S. waterways a “high priority” (U.S. EPA, 2015) and acknowledges that Nitrogen-Phosphorous (NP) pollution is a causal factor in algal blooms. However, the EPA’s 2015 report also notes that since many factors may contribute to a harmful algal bloom (HAB), “it is often difficult or impossible to say *how much more* likely an HAB is because of nutrient pollution.” Lack of experimental manipulation and small sample sizes are among many potential pitfalls in making causal inferences using stream surveillance data (Norton et al., 2014). The EPA’s Causal Analysis/Diagnosis Decision Information System (CADDIS) outlines a reasoned, methodical process for assessing causality in stream ecosystems (Norton et al., 2009). Suter et al. (2002), among the primary developers of CADDIS, state that data analysis methods in causal assessments “should be selected to best illuminate the association given the amounts and types of data available.” In this paper, a potential outcome (or counterfactual) approach is considered for drawing inference about the causal effects of nutrient pollution on stream ecosystems.

Data on North Carolina’s Cape Fear River is analyzed as a case study. This is a large Piedmont-Coastal Plain system that is representative of many riverine systems from Virginia south through North Florida (Dame et al., 2000). Formerly considered a moderately productive river (Kennedy and Whalen, 2007), in 2009 it began experiencing harmful algal blooms consisting of the cyanobacterium (blue-green alga) *Microcystis aeruginosa* near Lock and Dam 1 (LD1) that reappeared periodically through 2012 (Isaacs et al., 2014). Freshwater algal blooms are often stimulated by phosphorus (P) loading (Howarth and Marino, 2006), but in Coastal Plain rivers and streams, algal blooms are largely stimulated by nitrogen (N) loading (Mallin et al., 2004; Dubbs and Whalen, 2008). In North Carolina

(NCDENR, 2005) as well as many states and provinces, regulatory agencies regularly monitor concentration of the algal pigment chlorophyll a as a proxy for algal bloom strength. Long-term monitoring of this river by state-certified coalitions, including the Lower Cape Fear River Program and Middle Cape Fear Coalition, has provided a data set of nutrients, chlorophyll a , and other water quality parameters for the middle and lower river, where the blooms are concentrated.

This paper shows that causal effects of upstream nutrient concentrations on downstream chlorophyll a can be estimated from observational water quality data. Correlation analyses or regression techniques, while invaluable for exploring associations within an ecosystem, do not typically estimate causal effects. With publicly available watershed monitoring data, we assess causal effects of nutrient concentrations measured upstream of LD1 on chlorophyll a levels at LD1 by adapting the causal g-methods (Robins and Hernán, 2009; Hernán and Robins, 2018). Originally developed for assessing the effect of a time-varying exposure, here the g-methods are extended to the setting where exposure varies in both time and space. In particular, the causal models allow for spatial interference (Verbitsky-Savitz and Raudenbush, 2012; Di Gennaro and Pellegrini, 2016) in the sense that exposure (nutrient concentration) at one location may affect the outcome (chlorophyll a) at another location. Inference about parameters of marginal structural models, the parametric g-formula, and structural nested models which accommodate the spacetime interference structure of a stream ecosystem is considered using estimating equation theory (Stefanski and Boos, 2002), with small sample adjustments (Fay and Graubard, 2001) to account for limited independent replicates.

The paper is organized as follows. Section 2 motivates the analysis and describes the available data on the Cape Fear River. Section 3 introduces potential outcomes, key assumptions, and the target estimand. A graphical representation of the model assumptions

using a Single World Intervention Template (Richardson and Robins, 2013) is also presented. The g-methods are presented in Section 4 along with small sample variance corrections. The simulation study in Section 5 validates and compares statistical properties of the g-methods. The Cape Fear River data are analyzed in Section 6. Finally, we discuss our findings and their limitations in Section 7. The Supplementary Material contains the code and data necessary to replicate the analyses plus additional mathematical and analysis details.

2 Motivation, materials, and notation

2.1 Cape Fear River nutrient pollution and algal blooms

During the summers of 2009-2012, algal blooms unprecedented in scale and composition occurred near LD1 near Kelly, NC. Isaacs et al. (2014) reported that samples collected from these blooms in 2009 and 2012 consisted predominantly of toxic *Microcystis aeruginosa* cyanobacteria. The multi-stakeholder watershed action plan for the Cape Fear River identifies blue-green algae, *M. aeruginosa* in particular, as a significant threat to the river ecosystem (Cape Fear River Partnership, 2013). Over 2 million people rely on drinking water from the Cape Fear watershed, and algal blooms have impacted taste and odor from some water treatment plants (Ahuja, 2013). Brunswick County, in southeastern North Carolina, obtains some of its drinking water directly from the river near LD1. Taste and odor problems arising from the cyanobacterial blooms forced the water utility to increase its level of water treatment, at significant cost, to produce acceptable drinking water. Thus, causes of the recent degradation in Cape Fear River water quality are key management concerns.

The 9000 square mile Cape Fear watershed is contained entirely within the political boundaries of North Carolina, extends from Greensboro to Wilmington, and includes parts of Durham and Chapel Hill. The Cape Fear River forms at the confluence of the Haw and Deep Rivers and once supported rich fisheries of anadromous fish (Cape Fear River Partnership, 2013). Figure 1 shows the extent of the Cape Fear watershed and the area of interest for this study, the section of river from Fayetteville to LD1.

The Nature Conservancy of North Carolina obtained coalition-produced, state-certified data consisting of monthly measurements from locations throughout the Cape Fear basin from July 1996 through June 2013. Prior to 1999, chlorophyll *a* was not consistently measured at LD1. Since large blooms at LD1 were reported mainly during summer months, we focused our analysis on observations from June, July, August, and September of 1999 to 2012 from the main stem of the Cape Fear River upstream of LD1. The data include concentration measurements of four NP compounds (all in mg/L): nitrate (NO_3), ammonia (NH_3), total Kjeldahl nitrogen (TKN), and phosphorous (P).

2.2 Associations of nutrients and LD1 chlorophyll

A simple correlation analysis shows generally positive associations between upstream nutrients and chlorophyll *a* levels at LD1. Figure 2 plots Spearman's correlation coefficients between nutrient concentrations at sampling locations within the study region and LD1 chlorophyll *a*. Each nutrient has a slightly different trajectory over the course of the river, but with the exception of TKN, the correlation peaks between 65 and 95 river kilometers upstream of LD1. These associations suggest a relationship between upstream nutrient levels and LD1 chlorophyll. Our goal in this paper is to adjust for confounding to determine to what degree the upstream nutrients cause changes in LD1 chlorophyll *a*.

Figure 1: The map shows the extent of the Cape Fear watershed within the political boundaries of North Carolina, as well as the region of interest for this study. The algal blooms generally occurred near LD1. This study examines causal relationships between nutrient concentration measured at upstream sampling locations (open triangles) on chlorophyll *a* at LD1.

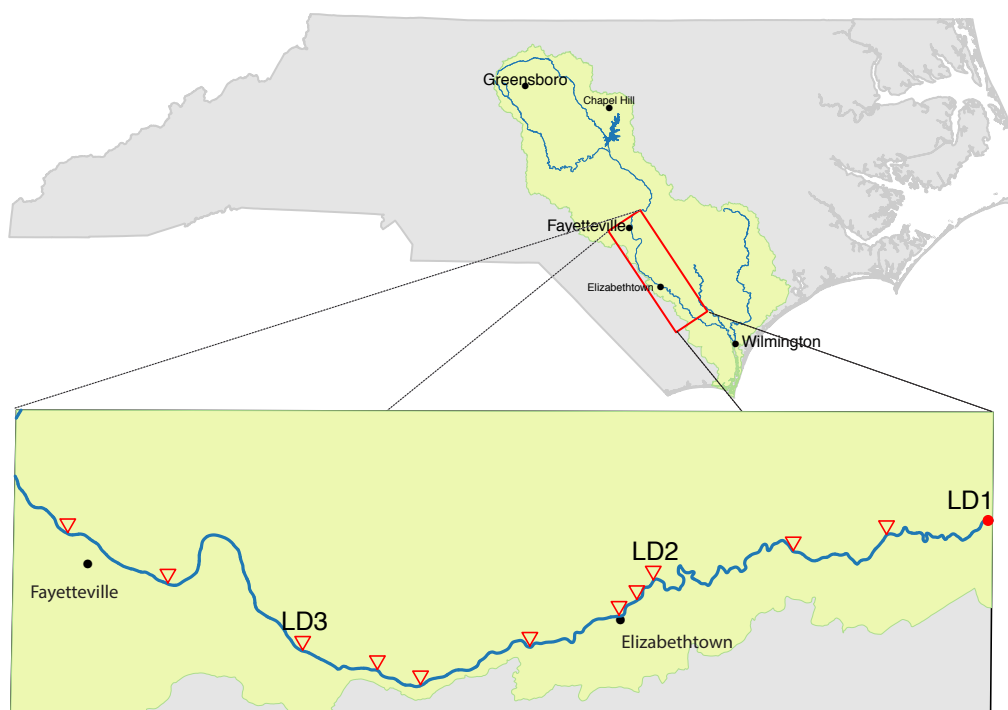
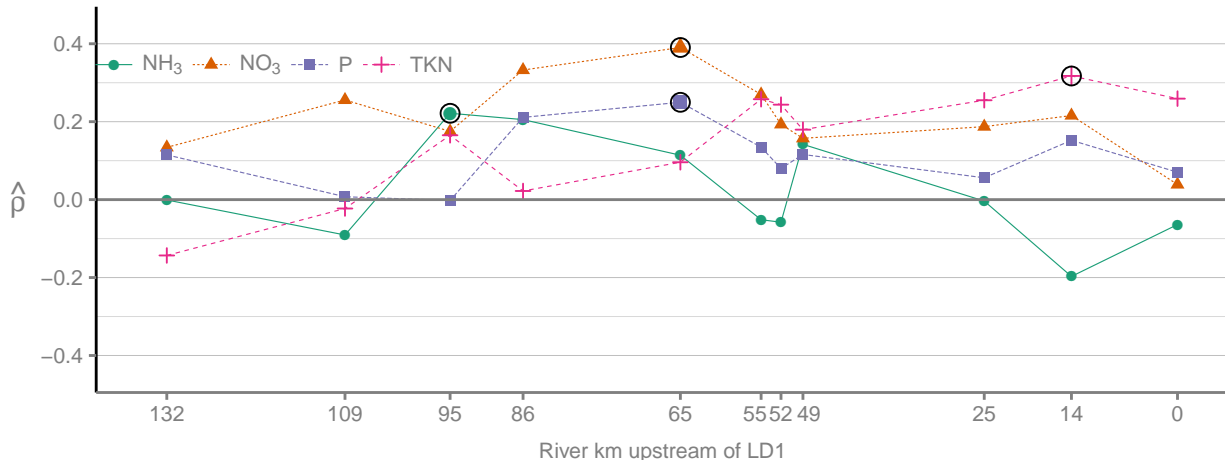


Figure 2: Spearman’s correlation coefficients between nutrient levels at upstream sampling locations and LD1 chlorophyll a , using observations from June-September of 1999-2012. Open circles indicate the maximum correlation for a nutrient within this reach of the river.



2.3 A mathematical description

Let $i = 1, \dots, m$ index independent replicates; for the Cape Fear data, $m = 14$ corresponding to the years 1999 to 2012. We assume that clusters of summer months are sufficiently far enough apart in time to be considered independent. That is, observations from June to September of year i are independent of the same set of observations in year $i' \neq i$, but observations within a year may be correlated. This is the “time-slices” approach recommended by CADDIS for relieving temporal autocorrelation¹. For a generic random variable W , the indexing W_{ist} is used where i indicates year, $s = 1, \dots, n_s$ indicates the sampling locations, ordered from upstream to downstream, and $t = 1, \dots, n_t$ indicates the month (e.g., $t = 1$ denotes June). In the following, the i notation is dropped where convenient. In general capital letters denote random variables and lower case letters denote indices,

¹<https://www.epa.gov/caddis-vol4/caddis-volume-4-data-analysis-basic-principles-issues>

constants, or possible values of random variables. The notation f_w or $f(w)$ is used as the probability density or mass function for a random variable W .

Observed values of chlorophyll a ($\mu\text{g/L}$), the outcome of interest, are \log_2 transformed and denoted as Y_{st} . For simplicity, chlorophyll a is referred to as chlorophyll in the following. The effect of each nutrient is considered separately in our analysis, and nutrient exposure is generically denoted as A_{st} . Other covariates measured concurrently with nutrient concentrations include the date and time of measurements, water temperature ($^{\circ}\text{C}$), dissolved oxygen, pH, and turbidity. In addition to covariates recorded in the water quality data set, daily mean discharge data from stream gauges located at the William O’Huske Lock and Dam (LD3) and LD1 were downloaded from USGS and converted to m^3/s . Discharge values were linearly interpolated based on river distance for sampling locations between the gauges. For each location, the average of the mean daily discharge from the same date as the water quality measurements plus the two prior days was used in the analysis. Let L_{st} denote covariates measured at location s in month t . Let $O_{st} = \{Y_{st}, A_{st}, L_{st}\}$ denote the observed random variables at location s in month t . For any variable W_{st} , let the $s \times t$ matrix \overline{W}_{st} denote the variable’s history for all locations upstream to and including location s , plus all time points prior to and including time point t .

3 Causal inference from upstream to downstream

Let $Y_{s^*t}(\overline{a}_{st})$ be the potential value of \log_2 chlorophyll at location s^* in month t had the exposure history been \overline{a}_{st} , for $s < s^*$. By causal consistency (Pearl, 2010), $Y_{s^*t}(\overline{a}_{st}) = Y_{s^*t}$ when $\overline{A}_{st} = \overline{a}_{st}$. Define the average potential outcomes for a location of interest s^* over months $t = 1, \dots, n_t$ as $\text{E}\{[Y_{s^*1}(\overline{a}_{s1}), Y_{s^*2}(\overline{a}_{s2}), \dots, Y_{s^*n_t}(\overline{a}_{sn_t})]^\top\} = \text{E}[Y_{s^*}(\overline{a}_s)]$. In the analysis, $s^* = 3$ corresponds with LD1.

3.1 Effects of interest

Nutrient effects of interest to policymakers or scientists (the estimands) can be stated in terms of functions of average potential outcomes. For example, what difference would be expected, on average, in LD1 chlorophyll levels if NH_3 exposure at the upstream points LD3 and LD2 was set to be above, rather than below, a certain threshold during the month of June ($t = 1$)? Letting s_1 correspond to LD3 and s_2 correspond to LD2, this estimand is, in the notation defined above, $E[Y_{31}((a_{11}, a_{21})^\top) - Y_{31}((a'_{11}, a'_{21})^\top)]$, where a_{11} and a_{21} indicate NH_3 exposure at LD3 and LD2 above the NH_3 threshold and a'_{11} and a'_{21} indicate NH_3 levels below the threshold.

Consider the estimand which measures the effect of setting nutrient concentrations at two upstream locations, s_1 and s_2 , on LD1 chlorophyll averaged across n_t months, i.e.,

$$\mu(a_t, a'_t) = \frac{1}{n_t} \sum_{t=1}^{n_t} E \{Y_{3t}(0_{t-1} : a_t) - Y_{3t}(0_{t-1} : a'_t)\}, \quad (1)$$

where 0_t is a $2 \times t$ matrix of zeros defined as the empty set when $t = 0$, $a_t = (a_{1t}, a_{2t})^\top$, and $R : Q$ indicates the concatenation of matrices R and Q . Note 0 without a subscript denotes the scalar zero. The estimand (1) is defined in general for any two exposure settings a_t and a'_t . In the Cape Fear River analysis, exposure is defined as a 2-tuple of binary variables both being above ($a_t = (1, 1)^\top$) or both below ($a'_t = (0, 0)^\top$) cutpoints specified in Section 6. For brevity, $\mu(a_t, a'_t)$ is denoted μ .

The estimand (1) characterizes the average effect on LD1 chlorophyll when intervening at two upstream locations simultaneously. This parameter is of interest to the community of scientists working on the Cape Fear River who want to understand the effects of nutrient concentrations from different upstream locations on LD1 chlorophyll during the summer when the toxic algal blooms generally occurred. Assessing the causal effect of exposures

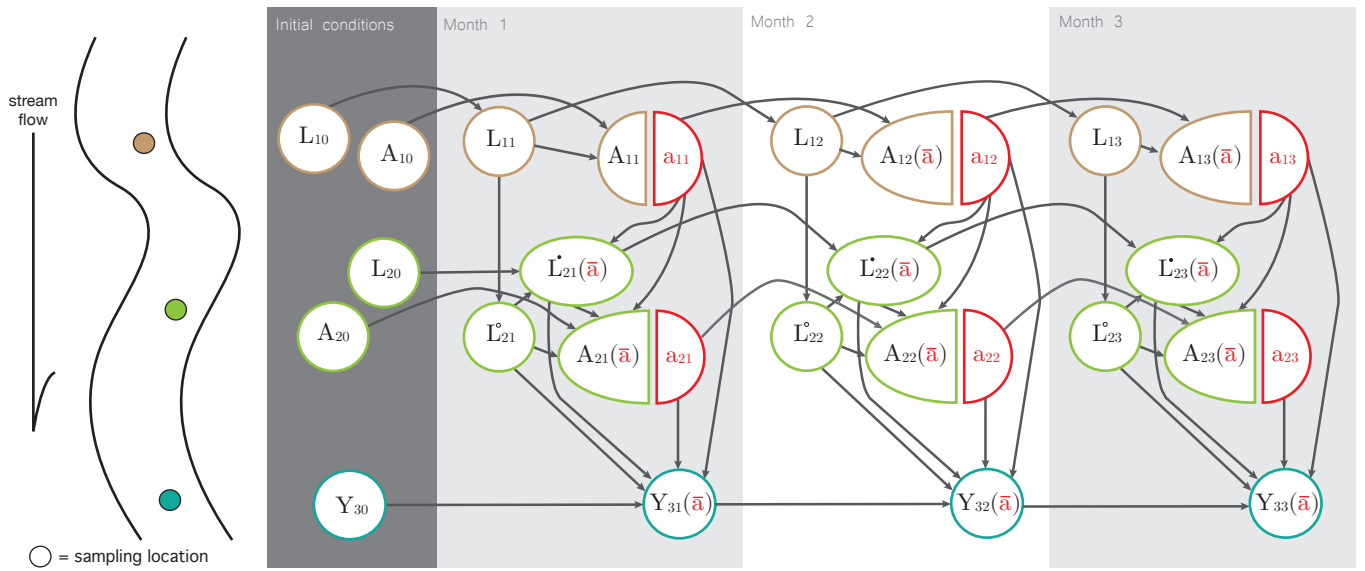
at two upstream locations simultaneously requires adjusting for covariates that affect the exposure and vary between the upstream locations. Not correctly accounting for such covariates may result in biased inferences about the nutrient effects.

3.2 Single world intervention graph

Richardson and Robins (2013) introduced single world intervention graphs (SWIGs) to unify the graphical approach to causal inference (e.g., see Pearl, 2009) and the more algebraic potential outcomes framework (e.g., see Rubin, 2005). An important difference between the approaches is the representation of potential outcomes. Algebraic notation can easily distinguish between potential and observed outcomes ($Y(a)$ versus Y). Directed acyclic graphs (DAGs) do not explicitly encode potential outcomes. SWIGs do.

Reading a SWIG is similar to reading a DAG. Nodes represent variables and edges suggest causal relationships between nodes (Figure 3). In a SWIG, however, intervention nodes are transformed by a node-splitting operation. Instead of a single A_{11} node as in a DAG, the A_{11} semicircle represents the random variable for exposure at location 1 at time 1. The a_{11} semicircle represents the fixed setting of the exposure (possibly contrary to fact) at the same spacetime point. Figure 3 is technically a single world intervention template (SWIT), not a SWIG. SWITs are a graphical template for a set of exposure levels, whereas SWIGs represent the graph for a single exposure level. We assume the SWIGs have the same form for all exposures and all their levels, hence a single SWIT describes the SWIGs for all exposure levels.

Figure 3: This single world intervention template conceptualizes the upstream to downstream process. A_{st} is an exposure of interest, and a_{st} is a fixed value of the exposure. At location 2, space-varying covariates labeled L_{2t}^\bullet are associated with the potential outcome $Y_{3t}(\bar{a})$, affect A_{2t} , and are affected by A_{1t} . L_{2t} covariates without the space-varying confounding properties are labeled L_{2t}° . Within nodes with random variables that depend on past history, \bar{a} is a generic history whose contents depend on s and t as described in the main text. This SWIT does not include all possible arrows. For example, $a_{1t} \rightarrow L_{2t}(\bar{a})$ would imply an effect of the exposure from the previous month and location. Since the strongest effects should occur within a month, temporal arrows are limited to the effects of covariates and exposures at the same node in the following month.



4 Estimation of causal effects

Time-varying confounding may introduce bias if not accounted for in estimation. Robins and Hernán (2009) describe three g-methods for estimating causal effects from observational data in the presence of time-varying confounding: the parametric g-formula, fitting marginal structural models (MSMs) using inverse probability weighting, and g-estimation of structural nested models (SNMs). This section describes extensions of these g-methods to the spacetime setting.

4.1 Causal assumptions

The causal effect μ can be identified by the distribution of the observable random variables by considering the structure of a stream (represented by Figure 3) as a sequentially and conditionally randomized experiment. Given (i) covariate values up to and including location s and month t and (ii) values of the past exposure(s) prior to location s and month t , A_{st} is assumed to be independent of the potential outcomes. That is, the covariate and exposure histories must block all back-door paths between A_{st} and $Y_{s^*t}(\bar{a}_{st})$ (Pearl, 2009), which implies conditional independence, commonly referred to as the strong ignorability or no unmeasured confounding assumption:

$$Y_{s^*t}(\bar{a}_{st}) \perp A_{st} \mid \bar{L}_{st}, \bar{A}_{st}^\dagger, \quad (\text{A1})$$

where $\bar{A}_{st}^\dagger = \bar{A}_{st} \setminus \{A_{st}\}$.

For the g-formula and MSMs, identification of causal effects also depends on a positivity assumption $f(a_{st} \mid \bar{O}_{st}^\dagger = \bar{o}_{st}^\dagger) > 0$ for all \bar{o}_{st}^\dagger such that $f(\bar{o}_{st}^\dagger) > 0$ where $\bar{O}_{st}^\dagger = \bar{O}_{st} \setminus \{A_{st}\}$. That is, each level of exposure must have some non-zero probability of occurring at all spacetime points for all possible covariate and exposure histories.

These assumptions are needed to identify causal effects nonparametrically. In many applications, as in ours, common finite-dimensional parametric models such as linear or logistic regression are employed to model aspects of the distribution of observable random variables. These models must be correctly specified in order for the resulting inferences to be valid.

4.2 Parametric g-formula

The g-formula is a mathematical identity which relates the distribution of counterfactuals to the distribution of the observable random variables (Robins, 1986; Robins and Hernán, 2009). For example, using the g-formula, the counterfactual mean can be expressed as:

$$E[Y_{s^*t}(\bar{a}_{st})] = \int_{\bar{l}_{st}} E[Y_{s^*t}|\bar{A}_{st} = \bar{a}_{st}, \bar{L}_{st} = \bar{l}_{st}] f_{\bar{l}_{st}} d\bar{l}_{st}. \quad (2)$$

where $f_{\bar{l}_{st}} = \prod_{j=1}^s \prod_{k=1}^t f_{l_{jk}|\bar{l}_{j-1,k-1}, \bar{a}_{j-1,k-1}}$. In practice, the mean model $E[Y_{s^*t}|\bar{A}_{st} = \bar{a}_{st}, \bar{L}_{st} = \bar{l}_{st}]$ and conditional densities or mass functions $f_{l_{jk}|\bar{l}_{j-1,k-1}, \bar{a}_{j-1,k-1}}$ are not known, and estimated values $\hat{E}[Y_{s^*t}|\bar{A}_{st} = \bar{a}_{st}, \bar{L}_{st} = \bar{l}_{st}]$ and $\hat{f}_{\bar{l}_{st}}$ are plugged into (2) to estimate $E[Y_{s^*t}(\bar{a}_{st})]$. Though these quantities may be estimated nonparametrically for a single spacetime point, a parametric approach may be necessary to estimate more complicated quantities such as μ . In both the analysis and simulations presented below, the mean model was parameterized as a linear model with main effects only for A_{2t} , A_{1t} , and L_{2t} , with corresponding parameters β_1^g , β_2^g , and β_4^g , respectively. Let γ_3^g be the parameter corresponding to A_{1t} in a simple linear model for the mean of L_{2t} . When the exposure settings are binary where $a_{st} = 1$ and $a'_{st} = 0$ for all t , then $\mu = n_t^{-1} \sum_{t=1}^{n_t} \{\beta_1^g + (\beta_2^g + \beta_4^g \gamma_3^g)\} = \beta_1^g + \beta_2^g + \beta_4^g \gamma_3^g$. The Supplementary Material contains the algebraic details. Maximum likelihood is used to estimate the model coefficients. The coefficient estimates are then plugged into (2) to

obtain the estimator of $E[Y_{s^*t}(\bar{a}_{st})]$.

One drawback to the parametric g-formula is the g-null paradox, wherein if the null hypothesis of no treatment (exposure) effect is true, plugging standard parametric models into (2) will result in rejection of this null (Robins and Hernán, 2009) as sample size increases. The inferential approaches in the next two sections do not suffer the g-null paradox.

4.3 Marginal structural model

Marginal structural models posit a parametric relationship between an exposure history and a counterfactual outcome. Consider the following MSM:

$$E[Y_{s^*t}(\bar{a}_{st})] = \beta_{0t}^m + \beta_1^m a_{st} + \beta_2^m a_{s-1,t}. \quad (3)$$

Each month may have a distinct intercept β_{0t}^m , but the counterfactual mean depends only on exposure at two upstream locations during the same month. From (3), $\mu = \beta_1^m + \beta_2^m$. Parameters in MSMs can be estimated consistently using inverse probability weighting methods (Hernán et al., 2000). We use the stabilized inverse probability weight where each observed outcome is weighted by:

$$SW_{st} = \prod_{j=1}^s \prod_{k=1}^t \frac{f(a_{jk} | \bar{A}_{jk}^\dagger = \bar{a}_{jk}^\dagger)}{f(a_{jk} | \bar{O}_{jk}^\dagger = \bar{o}_{jk}^\dagger)}. \quad (4)$$

The product is taken across the dimensions of space s and time t as opposed to a single dimension as in Robins et al. (2000). Logistic regression is used to estimate $f(a_{st} | \bar{A}_{st}^\dagger = \bar{a}_{st}^\dagger)$ and $f(a_{st} | \bar{O}_{st}^\dagger = \bar{o}_{st}^\dagger)$ (see Supplementary Materials for details). Weighting observed outcomes by (4), generalized estimating equations (GEE) (Liang and Zeger, 1986) with an independence working correlation matrix are used to estimate $\beta^m = (\beta_0^m, \beta_1^m, \beta_2^m)$.

4.4 Structural nested (mean) model

Instead of modeling counterfactual means from which causal contrasts are then derived, structural nested models directly model a causal effect (Robins, 1994). In general, SNMs model the effect of removing treatment (exposure) within strata l , $E[Y(a) - Y(0)|L = l]$. Vansteelandt and Joffe (2014) describe several advantages of SNMs over MSMs. For one, target parameters in SNMs are identified without the positivity assumption. The asymptotic variance of IPW estimators also tends to be more sensitive to misspecification of the model(s) compared to G-estimators of SNM parameters (Vansteelandt and Joffe, 2014). SNMs can also be used to test the null hypothesis of no effect for *any* treatment regime, which MSMs cannot do (Robins, 2000).

The Cape Fear River analysis uses the following structural nested mean model:

$$\begin{bmatrix} \vdots \\ E \left\{ Y_{3t} \begin{pmatrix} a_{1t} \\ 0_t \end{pmatrix} - Y_{3t} \begin{pmatrix} a_{1t} \\ 0 \end{pmatrix} \middle| \bar{L}_{2t} = \bar{l}_{2t} \right\} \\ E \left\{ Y_{3t} \begin{pmatrix} a_{1t} \\ 0_t \end{pmatrix} - Y_{3t} \begin{pmatrix} 0 \\ 0_t \end{pmatrix} \middle| \bar{L}_{1t} = \bar{l}_{1t} \right\} \\ \vdots \end{bmatrix} = \begin{bmatrix} \vdots \\ h_{1t}(\bar{a}_t, \bar{l}_{2t}; \beta^s) \\ h_{2t}(\bar{a}_t, \bar{l}_{1t}; \beta^s) \\ \vdots \end{bmatrix} = \begin{bmatrix} \vdots \\ \beta_1^s a_{2t} \\ \beta_2^s a_{1t} \\ \vdots \end{bmatrix}. \quad (5)$$

For $n_t = 4$, (5) has dimension 8×1 , as each month t has two h functions. The h function corresponds to a “blip down” process (Vansteelandt and Joffe, 2014), removing the effect of treatment one spatial location at a time. The first h_{1t} “blips out” and quantifies the effect of a_{2t} , and h_{2t} quantifies the effect of a_{1t} . This SNM assumes that h does not depend on l ; that is, the causal contrast does not include interactions between exposure and covariates. Thus, $\beta_1^s + \beta_2^s = \mu$. While in general a SNM can include interactions between exposures

and spacetime-varying confounding covariates, we specify (5) with no interactions in order for μ to equal a simple linear function of the SNM parameters.

To estimate β^s , a vector $U_t(\beta^s)$ is constructed whose mean value, given \bar{L}_{st} and \bar{A}_{st} , equals the mean outcome that would have been observed had treatment been removed:

$$U_t(\beta^s) = \begin{pmatrix} U_{1t}(\beta^s) \\ U_{2t}(\beta^s) \end{pmatrix} = \begin{pmatrix} Y_{3t} - \beta_1^s A_{2t} \\ Y_{3t} - (\beta_1^s A_{2t} + \beta_2^s A_{2,t-1}) \end{pmatrix}.$$

Using a modified version of equation (33) in Vansteelandt and Joffe (2014), the solution to the following estimating equations is a consistent estimator for β^s :

$$\sum_i \sum_{s=1}^{n_s} \sum_{t=1}^{n_t} [d_s(\bar{L}_{ist}, \bar{A}_{ist}) - E\{d_s(\bar{L}_{ist}, \bar{A}_{ist}) | \bar{L}_{ist}, \bar{A}_{ist}\}] [U_{ist}(\beta^s) - E\{U_{ist}(\beta^s) | \bar{L}_{ist}, \bar{A}_{ist}\}] = 0, \quad (6)$$

where d_s is some arbitrary distance function. Per the suggestion of Vansteelandt and Joffe (2014), we let $d_s = E\{\partial U_{st}(\beta)/\partial \beta | \bar{L}_{st}, \bar{A}_{st}\}$. The solution to (6) is called a G-estimator and has the advantage of double robustness. That is, the estimator is consistent when either the model for the transformed outcome $E[U_{st}(\beta) | \bar{L}_{st}, \bar{A}_{st}]$ or the exposure model (which is a component of $E[d_s(\bar{L}_{st}, \bar{A}_{st}) | \bar{L}_{st}, \bar{A}_{st}]$) is correctly specified. Parametric regression models were used to model both the outcome and exposure (linear and logistic regression, respectively). In some cases, solving (6) yields a closed form solution for $\hat{\beta}^s$ as shown in the Supplementary Material, which simplifies computations and makes the solution's uniqueness easy to check.

4.5 Estimating equation inference

In each of the previous three sections, the g-formula (2), MSM (3), and SNM (5) were specified such that parameter estimates may be obtained by solving a set of unbiased estimating equations. Therefore, under certain regularity conditions, the estimators will be consistent and asymptotically normal, and the empirical sandwich variance estimator can be used to consistently estimate the asymptotic covariance matrix of the model parameter estimators. In the case of the g-formula, the target estimand μ is a function of β_1^g , β_2^g , β_4^g , and γ_3^g , so the estimated variance of $\hat{\mu}$ can be obtained using the delta method. For MSMs, observed outcomes for each time point are weighted by estimated values of (4), and weighted generalized estimating equations are used to obtain $\hat{\beta}^m$. Variance estimates for MSMs can be obtained by stacking the score equations for the parametric models used to estimate the weights plus the estimating equations corresponding to (3) weighted by (4). Point estimates in the SNM were obtained from the closed form of $\hat{\beta}^s$, while variance estimates were obtained by stacking the score equations of both the outcome and exposure models along with estimating equation (6).

For all three methods, consistent variance estimators follow from estimating equations (i.e., M-estimation) theory (Stefanski and Boos, 2002). Let $\hat{\theta}$ be the estimator that solves the set of p equations $\sum_{i=1}^m g(O_i, \hat{\theta}) = 0$, where g is a vector of functions of length p corresponding to the number of parameters in θ . From our causal models, θ contains the target parameters β plus any nuisance parameters present in estimating the IP weights, outcome model, or exposure model. The asymptotic covariance for $\hat{\theta}$ is $\Sigma = A^{-1}B\{A^{-1}\}^\top/m$, where $A_i = \partial g(O_i, \theta)/\partial\theta$, $A = E[A_i]$, $B_i = g(O_i, \theta)g(O_i, \theta)^\top$, and $B = E[B_i]$. The empirical sandwich variance estimator replaces the expectations with their empirical counterparts and θ with $\hat{\theta}$; e.g., $\hat{A} = m^{-1} \sum_{i=1}^m \partial g(O_i, \theta)/\partial\theta|_{\theta=\hat{\theta}}$.

The empirical sandwich variance estimator is asymptotically consistent but tends to

underestimate the true variance in small samples (Fay and Graubard, 2001; Li and Redden, 2015). In the next section, we examine the bias corrected estimator of Fay and Graubard (2001) in simulations. The bias corrected variance estimator replaces \hat{B}_i with $\hat{B}_i^{bc}(b) = \hat{H}_i(b)\hat{B}_i\hat{H}_i(b)^\top$ to form $\hat{\Sigma}^{bc} = \hat{A}^{-1}\hat{B}^{bc}(b)\{\hat{A}^{-1}\}^\top$, where $\hat{H}_i(b) = \{1 - \min(b, \{\hat{A}_i\hat{A}\}_{jj})\}^{-1/2}$ and $\{\hat{A}_i\hat{A}\}_{jj}$ denotes the jj th element of $\hat{A}_i\hat{A}$ and $\hat{B}^{bc}(b) = \sum_i \hat{B}_i^{bc}(b)$. The constant b is less than 1 and chosen by the analyst intended to prevent extreme corrections when $\hat{A}_i\hat{A}$ is close to 1. Fay and Graubard (2001) “arbitrarily” set $b = 0.75$. To explore the stability of our variance estimates we used $b = 0.1, 0.3$, and 0.75 . Variance estimates were used to construct Wald confidence intervals based on either a normal distribution or a t distribution with m degrees of freedom.

5 Simulation study

Based on the SWIT in Figure 3, we used the `simcausal` R package (Sofrygin et al., 2016) to simulate data for $m = 10, 15, 20, 25$, and 30 years. For each m , 24,000 data sets were generated according to the parametrization provided in the Supplementary Material. The parameter values were based on estimates from simple linear or logistic regressions using the Cape Fear data with $\text{NO}_3 > 1$ mg/L as the exposure. For each simulated data set, estimates and 90% confidence intervals of μ were computed using the causal g-methods, plus a naive GEE approach that ignores space- and time-varying confounding. Code for the simulations is available in the Supplementary Material.

Figure 4 shows the absolute bias of the four estimators and empirical coverage of the corresponding confidence intervals for each set of simulations. The horizontal shading highlights bias < 0.01 , and the vertical shading highlights coverage within 1% of the nominal 90% coverage. Each facet in the figure shows a different correction to the variance estimator

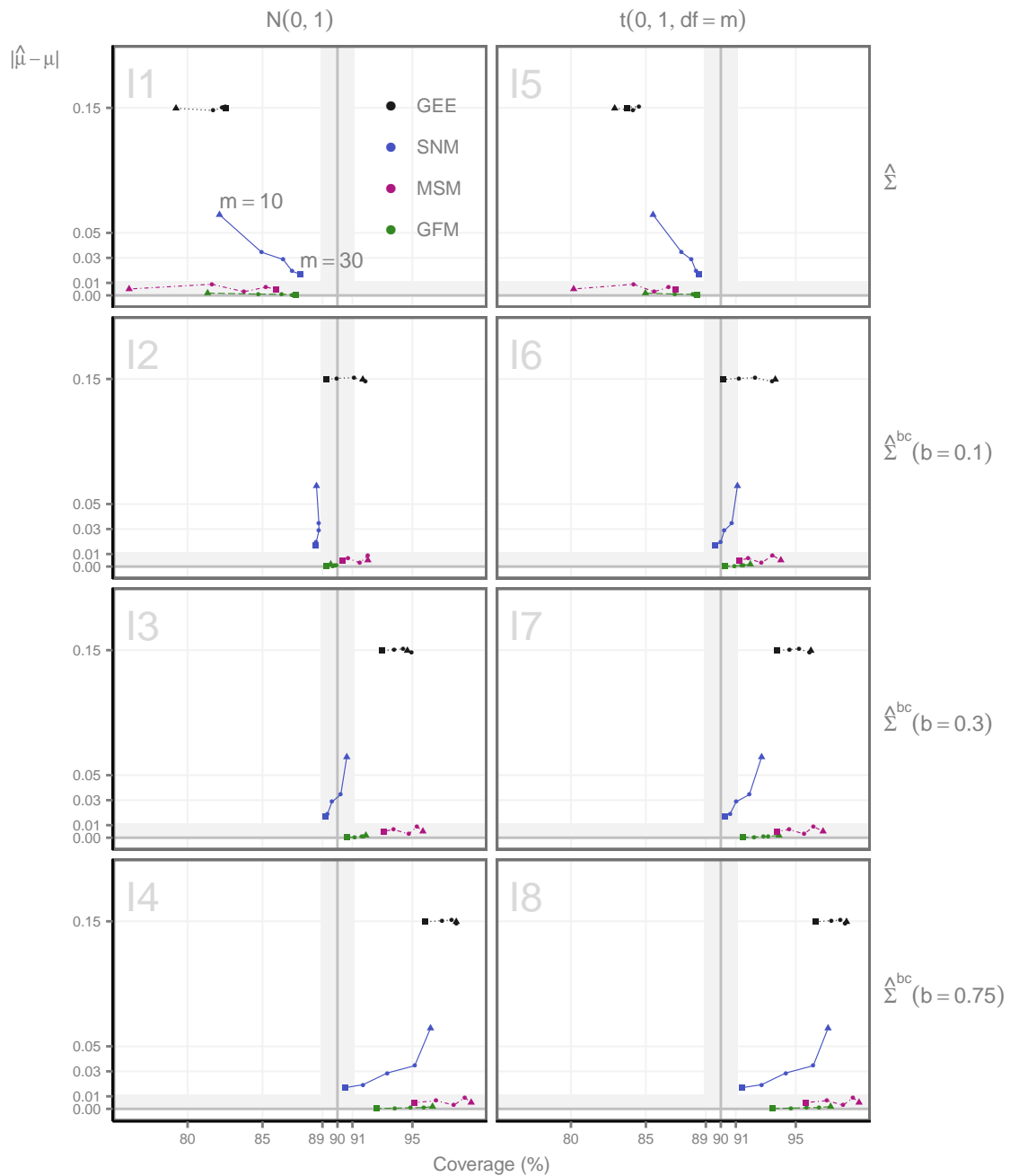
and distribution used in constructing the Wald confidence intervals. For all three causal methods, the absolute bias shrinks and the coverage improves as sample size (i.e., number of years) increases. The bias for the MSM and g-formula (GFM) methods is smaller compared to the SNM for all m analyzed in Figure 4. The SNM still has an average absolute bias of about 0.01 even when $m = 30$. In a secondary simulation of 1000 data sets where $m = 150$ (not shown), the SNM bias shrunk to the same order of magnitude as the MSM and g-formula methods. The naive GEE estimator is always biased, empirically illustrating why methods that account for time- and/or space-varying confounding should be used when such effects are present. For small m , the unadjusted variance estimator performs poorly, with Wald confidence intervals covering in the 75 - 85% range for all the methods (panels I1 and I5 in Figure 4). Larger values of b tend to overcorrect the variance estimate, but confidence interval coverage with $b = 0.1$ approximates the nominal level.

6 Cape Fear River analysis

Beginning with the sampling location 132 km upstream near I-95 in Fayetteville, we estimate μ for a given NP species at that site ($s = 2$) and the site just upstream ($s = 1$). That is, the causal effect was estimated for setting an exposure at location A and location B, then the effect of location B and location C, then the effect of location C and D, and so on downstream until the last sampling location upstream of LD1.

The methods described above treat exposures as binary, but the species of NP are measured on a continuous scale. For each species and set of upstream locations, the exposures were discretized using three cutpoints based on the 1st, 2nd and 3rd quartiles at the two upstream locations during April to October of 1999. The distribution for each NP species varied over the course of the river, so a single river-wide cutpoint would not

Figure 4: Simulation results show absolute bias $|\hat{\mu} - \mu|$ on the y-axis. Each line shows results for a method from $m = 10$ (triangle) to $m = 30$ (square). The proportion of simulations where the 90% confidence interval included the true value is shown on the x-axis. Each box shows results for the different methods of forming confidence intervals, with the columns defining the distribution and the row defining the form of the variance estimator. The bias is unaffected by corrections to the confidence intervals, hence the y-coordinates do not change across the boxes.



be meaningful. At some locations, for example, all the observed concentrations could be below a river-wide cutpoint. For each nutrient, five space-varying confounding covariates were considered: each of the other three nutrients, dissolved oxygen, or pH.

In summary, 40 causal effects were estimated (4 NP species \times 10 sets of s_2 and s_1 upstream locations) using each of the four different analysis methods (g-formula, MSM, SNM, and GEE). On the continuum from exploratory to confirmatory science, we view these results as exploratory causal analysis. For this reason, no control for multiple comparisons was made, and in the spirit of a pilot study (Lee et al., 2014), 90% confidence intervals are presented. Due partly to the small sample size and the simplified model (Figure 3) of a complex ecological web, these results do not confirm the magnitude and direction of causal effects; instead, these results should both be interpreted in light of existing evidence and inform future research.

The stability (*sensu* Rosenbaum, 2002) of these results was assessed by estimating the effects for each of three exposure cutpoints, five space-varying confounding covariates, and two different parameterizations of the outcome and exposure models. The stability analyses are summarized in the Supplementary Materials. Wald confidence intervals and p-values were computed using the eight combinations of distribution and variance estimator as in Figure 4. For each analysis method, the outcome and exposure models were parameterized similarly to the simulations, with the exception that L_{st}^o was not a single covariate and instead both temperature and discharge were included in the models.

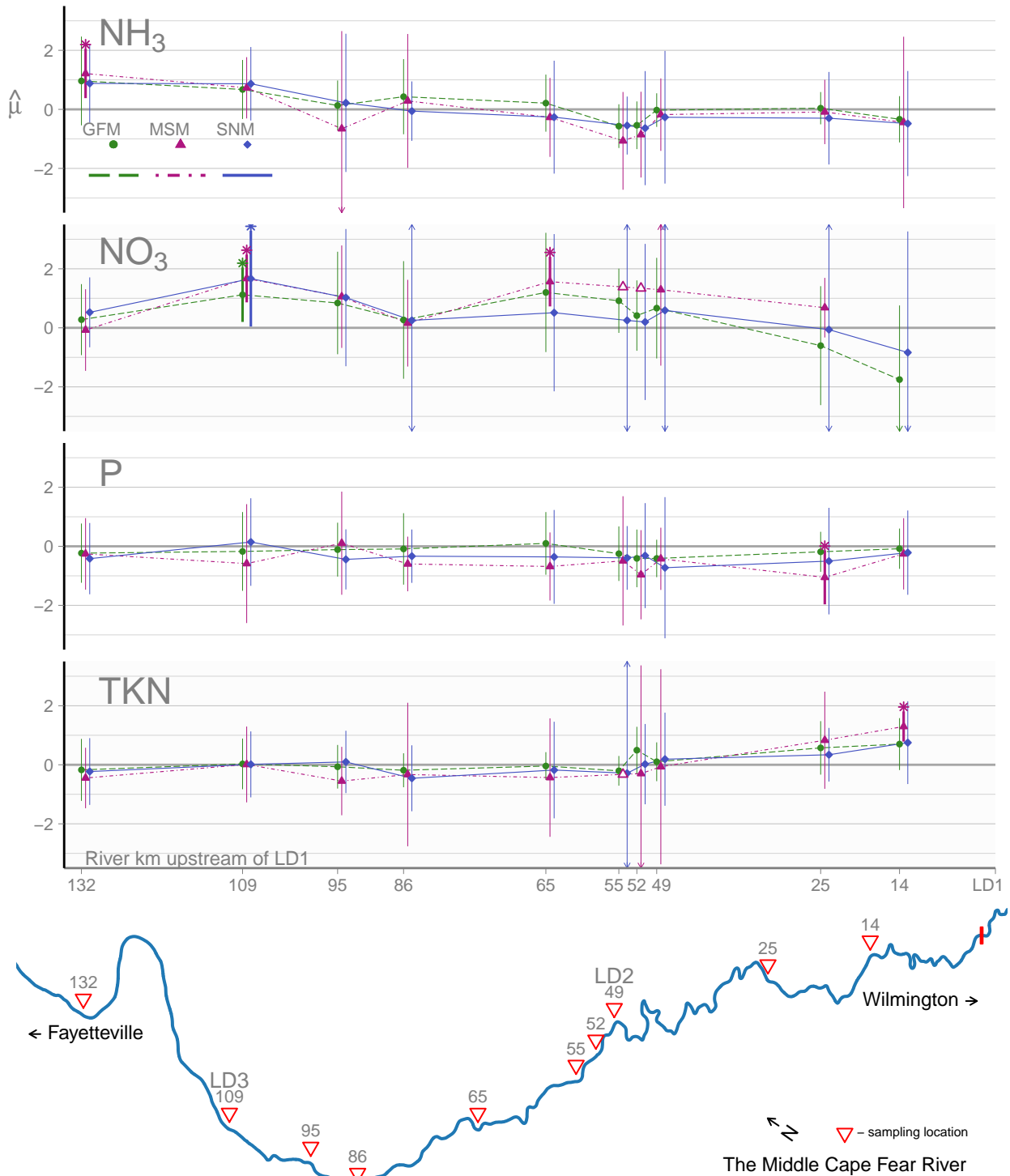
For the observations considered in our analysis, at most 5% of the data were missing for any given covariate. LD1 chlorophyll values were missing for May 2000 and July 2004. These two missing values were replaced by taking the average from the month prior and post. Of the 770 observations for the 11 upstream locations during May to September of 1999 to 2012, 5 NH_3 , 5 NO_3 , 22 TKN, 38 P, and 16 temperature values were missing.

No NH_3 or NO_3 were missing for June to September. Where possible, missing covariate values at a location-month were singly imputed in the following sequential manner. First, we attempted to average the values immediately upstream and immediately downstream during the same month. If either value immediately upstream or immediately downstream was missing, then we averaged values from the next site upstream and next site downstream during the same month. If neither of these approaches imputed a value, then we averaged the prior month and next month from the same location. This approach imputed missing values for all nutrient covariates except P, which had missing values for all summer months at all of our upstream locations in 2009. We excluded 2009 in analyses involving P. The stability of this simple approach to missing data was checked using a multiple imputation procedure (Harrell Jr et al., 2017), which is described in the Supplementary Materials. The results in Figure 5 do not substantively change with the multiple imputation.

Figure 5 shows causal effect estimates with point-wise 90% confidence intervals for the four nutrient species using the median cutpoint for the exposure as described above. To be conservative, the confidence intervals are based on $\hat{\Sigma}(b = 0.3)$. GEE and g-formula results were largely similar, so we only show g-formula results. Although the GEE and g-formula results were alike for these data, this will not be the case in general as demonstrated in the simulation study in Section 5. The space-varying covariate is P for the nitrogen species, and it is NH_3 for P. In this set of analyses, one of the models for the terms in (4) failed to converge when estimating the MSM in four cases (three for NO_3 and one TKN). These are indicated by open points, which were interpolated from the other values, unless the model failed for the location just upstream of LD1. Confidence intervals are based on the bias corrected standard errors ($b = 0.3$) and a t -distribution with m degrees of freedom. Thick bars with stars above indicate confidence intervals which exclude the null value of 0.

The point estimates of the three causal methods tend to have similar results. Standard

Figure 5: Results of causal analysis of Cape Fear River data from June-September of 1999-2012 for each of the four measured nutrients. Points are estimates of μ . Vertical lines are 90% confidence intervals with thicker lines highlighting intervals that do not cross zero. The intervals used in this plot use method I7 of Figure 4. Open points are where the model fitting algorithm failed to converge.



errors were also of similar magnitude, with the exception of estimates when s_2 is LD2 where the standard errors for the SNM tended to be uninformative. All three methods indicate a statistically significant effect of NO_3 when s_2 is the LD3 sampling location, 109 kilometers upstream of LD1. The point estimates at this location for NO_3 were 1.12 for the g-formula and 1.67 for the MSM and SNM, implying a 2- to 3-fold increase in LD1 chlorophyll when NO_3 is above 0.38 mg/L at both the location 109km upstream (LD3) and the location 132km upstream (near Cross Creek waste water treatment plant). Effect estimates of NH_3 , P and TKN consistently hover near zero with two exceptions. The effect of NH_3 appears to decrease after 109km upstream, and the effect of TKN appears to increase after 49km upstream.

The Supplementary Material includes summaries of results for all cutpoints, space-varying confounding covariates, test statistic distribution settings, as well as multiple outcome and exposure model specifications. Point estimates varied modestly depending on the cutpoint, space-varying confounding covariate, and how the exposure/outcome models were specified. All of the point estimates for NO_3 were greater than zero for locations 109, 95, and 86 kilometers upstream. Statistical significance was sensitive to the choice of Wald test statistic distribution but generally accords with the shifts in significance seen in the simulation results.

7 Discussion

Our results corroborate existing evidence that the much more abundant nitrate form of N is a major driver of downstream chlorophyll production in the middle section of the Cape Fear River. Among dissolved inorganic N species, cyanobacteria prefer to assimilate N in the form of ammonium and then switch to nitrate uptake when ammonium is depleted

(Burkholder, 2002). In this section of the Cape Fear River, ammonium is typically at low concentrations while nitrate concentrations are an order of magnitude higher (Mallin et al., 2006; Kennedy and Whalen, 2007). Experimental additions of inorganic and organic N have stimulated algae growth in the Cape Fear River (Dubbs and Whalen, 2008) and its two major tributaries, the Black and Northeast Cape Fear Rivers (Mallin et al., 2004). As cyanobacteria are a primary harmful algal taxa group of concern in this system, it is notable that N stimulates growth of this group (Burkholder, 2002) as well as growth of *Microcystis* specifically (Paerl, 1987; Siegel et al., 2011; Yuan et al., 2014).

Both point and nonpoint sources such as agricultural runoff contribute to nutrient concentrations in the Cape Fear River (Rajbhandari et al., 2015). Our data cannot distinguish between sources of pollution. While the data also cannot precisely pinpoint locations of nutrient inputs into the river, our analysis does indicate areas for further investigation. Across our choices of cutpoints and various exposure and outcome models (see Supplementary Material for details), significant effects of NO_3 tended to occur between 86 and 109km upstream of LD1. Notably, four major National Pollutant Discharge Elimination System permits are located in this reach of the river: the Tarheel Plant (NC0078344), Dupont Fayetteville Works (NC0003573), Cedar Creek Site (NC0003719), and the Rockville Creek Waste Water Treatment plant (NC0050105).

We have shown how “what if” questions on water quality of scientific and policy interest can be mathematically framed as causal estimands. In the presence of space- and/or time-varying confounding, this must be accounted for in estimation, else biased estimates will result. Our application is one of the first to use the g-methods (Robins and Hernán, 2009) as part of an ecological causal assessment. In fact, despite their general utility, structural nested models have rarely been applied in practice (Vansteelandt and Joffe, 2014). We demonstrate how they can be implemented and give details for deriving a closed form

estimator in the Supplementary Material.

Results from observational studies can always be skeptically reviewed, but the potential outcomes framework forms a basis for constructive critique. The causal assumptions described in Section 4.1 must be thoroughly vetted. Has all confounding been accounted for? Are the parametric forms of our models correctly specified, or reasonably so? Various criteria have been proposed to assess fit of marginal structural models (Platt et al., 2013; Baba et al., 2017), and methods such those described in Wang et al. (2006) may be used to check sensitivity of IPW estimators. As a diagnostic of the g-formula model fit, Westreich et al. (2012) suggest estimating the outcome distribution based on the “natural course” of exposure, which should be comparable the observed outcome distribution. While developed in the context of inferring optimal dynamic treatment regimes, Rich et al. (2010) and Henderson et al. (2010) proposed methods for assessing fit based on residuals of the models within a structural nested model.

As with any research, the causal effects estimated from a single analysis should not be the sole source of evidence. The methods described in this paper can augment assessment and decision frameworks such as the EPA’s CADDIS. The potential outcomes framework is well suited to aid policymakers in development of permit standards and surface water standards. Yuan (2010), for example, estimated effects of nutrient pollution on stream invertebrates using propensity score methods.

Lastly, while GEE methods are available in several R packages (Halekoh et al., 2006; Carey et al., 2015), generic M-estimation is not straightforward with current statistical software. The causal models implemented in this paper involve combining estimating equations from several models. The R package `geex` was developed in conjunction with this research to streamline a programmer’s work in implementing estimating equation theory. The Supplementary Material includes the code to replicate our analyses, and examples of `geex` for

causal models may be found therein.

SUPPLEMENTARY MATERIAL

Appendices: Four appendices containing additional explication of the g-formula, derivation of the closed form structural nested model estimators, details on simulations parameterizations, and additional analyses of Cape Fear River data. (PDF file)

R-package updown: R-package updown containing code to perform the simulations and analyses described in this paper. (GNU zipped tar file)

R-package geex: R-package geex containing code necessary for sandwich variance estimators used in updown package. (GNU zipped tar file)

R-package capefear: R-package capefear containing data from the Cape Fear River obtained by the North Carolina Nature Conservancy. Also contains discharge data from USGS stream gauges for the period of the study. (GNU zipped tar file)

References

- Ahuja, S. (Ed.) (2013). *Monitoring Water Quality: Pollution Assessment, Analysis, and Remediation*. Amsterdam; Boston: Elsevier.
- Baba, T., T. Kanemori, and Y. Ninomiya (2017). A criterion for semiparametric causal inference. *Biometrika* 104(4), 845–861.
- Burkholder, J. M. (2002). Cyanobacteria. In G. Bitton (Ed.), *Encyclopedia of Environmental Microbiology*, pp. 952–982. New York: Wiley.

- Cape Fear River Partnership (2013). Cape Fear River basin action plan for migratory fish. Technical report.
- Carey, V. J., T. Lumley, and B. Ripley (2015). *gee: Generalized Estimation Equation Solver*. R package version 4.13-19.
- Dame, R., M. Alber, D. Allen, M. Mallin, C. Montague, A. Lewitus, A. Chalmers, R. Gardner, C. Gilman, and B. Kjerfve (2000). Estuaries of the south Atlantic coast of North America: their geographical signatures. *Estuaries* 23(6), 793–819.
- Di Gennaro, D. and G. Pellegrini (2016). Policy evaluation in presence of interferences: A spatial multilevel DID approach. Technical report, CREI Working Paper No. 4/2016. Centro di Ricerca Interdipartimentale di Economia delle Istituzioni (CREI), University of Rome.
- Dodds, W. K., W. W. Bouska, J. L. Eitzmann, T. J. Pilger, K. L. Pitts, A. J. Riley, J. T. Schloesser, and D. J. Thornbrugh (2009). Eutrophication of U.S. freshwaters: Analysis of potential economic damages. *Environmental Science & Technology* 43(1), 12–19.
- Dubbs, L. L. and S. C. Whalen (2008). Light-nutrient influences on biomass, photosynthetic potential and composition of suspended algal assemblages in the Middle Cape Fear River, USA. *International Review of Hydrobiology* 93(6), 711–730.
- Fay, M. P. and B. I. Graubard (2001). Small-sample adjustments for Wald-type tests using sandwich estimators. *Biometrics* 57(4), 1198–1206.
- Halekoh, U., S. Hojsgaard, and J. Yan (2006). The R package geepack for generalized estimating equations. *Journal of Statistical Software* 15(2), 1–11.

- Harrell Jr, F. E., with contributions from Charles Dupont, and many others. (2017). *Hmisc: Harrell Miscellaneous*. R package version 4.0-3.
- Henderson, R., P. Ansell, and D. Alshibani (2010). Regret-regression for optimal dynamic treatment regimes. *Biometrics* 66(4), 1192–1201.
- Hernán, M. A., B. Brumback, and J. M. Robins (2000). Marginal structural models to estimate the causal effect of zidovudine on the survival of HIV-positive men. *Epidemiology* 11(5), 561–570.
- Hernán, M. A. and J. M. Robins (2018). *Causal Inference*. Boca Raton: Chapman & Hall/CRC, forthcoming.
- Howarth, R. W. and R. Marino (2006). Nitrogen as the limiting nutrient for eutrophication in coastal marine ecosystems: evolving views over three decades. *Limnology and Oceanography* 51(1part2), 364–376.
- Isaacs, J. D., W. K. Strangman, A. E. Barbera, M. A. Mallin, M. R. McIver, and J. L. Wright (2014). Microcystins and two new micropeptin cyanopeptides produced by unprecedented *Microcystis aeruginosa* blooms in North Carolina’s Cape Fear River. *Harmful Algae* 31, 82–86.
- Kennedy, J. T. and S. C. Whalen (2007). Seasonality and controls of phytoplankton productivity in the Middle Cape Fear River, USA. *Hydrobiologia* 598(1), 203–217.
- Lee, E. C., A. L. Whitehead, R. M. Jacques, and S. A. Julious (2014). The statistical interpretation of pilot trials: Should significance thresholds be reconsidered? *BMC Medical Research Methodology* 14(41).

- Li, P. and D. T. Redden (2015). Small sample performance of bias-corrected sandwich estimators for cluster-randomized trials with binary outcomes. *Statistics in Medicine* 34(2), 281–296.
- Liang, K.-Y. and S. L. Zeger (1986). Longitudinal data analysis using generalized linear models. *Biometrika* 73(1), 13–22.
- Mallin, M. A., V. L. Johnson, S. H. Ensign, and T. A. MacPherson (2006). Factors contributing to hypoxia in rivers, lakes, and streams. *Limnology and Oceanography* 51(1part2), 690–701.
- Mallin, M. A., M. R. McIver, S. H. Ensign, and L. B. Cahoon (2004). Photosynthetic and heterotrophic impacts of nutrient loading to blackwater streams. *Ecological Applications* 14(3), 823–838.
- NCDENR (2005). Cape Fear River basinwide water quality plan. Technical report, North Carolina Department of Environment and Natural Resources, Division of Water Quality/Planning, Raleigh, NC.
- Norton, S. B., S. M. Cormier, and G. W. Suter, II (2014). *Ecological Causal Assessment*. CRC Press.
- Norton, S. B., S. M. Cormier, G. W. Suter, II, K. Schofield, L. Yuan, P. Shaw-Allen, and C. R. Ziegler (2009). CADDIS: the causal analysis/diagnosis decision information system. In *Decision Support Systems for Risk-Based Management of Contaminated Sites*, pp. 1–24.
- Paerl, H. W. (1987). Dynamics of blue-green algal (*Microcystis aeruginosa*) blooms in the Lower Neuse River, NC: causative factors and potential controls. Technical Report 177.

- Pearl, J. (2009). *Causality*. Cambridge: Cambridge University Press.
- Pearl, J. (2010). On the consistency rule in causal inference: Axiom, definition, assumption, or theorem? *Epidemiology* 21(6), 872–875.
- Platt, R. W., M. A. Brookhart, S. R. Cole, D. Westreich, and E. F. Schisterman (2013). An information criterion for marginal structural models. *Statistics in Medicine* 32(8), 1383–1393.
- Rajbhandari, N. B., S. Pradhan, M. Di Luzio, A. Kebede, and V. Baker (2015). Identifying nutrient contributors in North Carolina’s Coastal Plain blackwater rivers. *American Journal of Environmental Sciences* 11(4), 313.
- Rich, B., E. E. Moodie, D. A. Stephens, and R. W. Platt (2010). Model checking with residuals for g-estimation of optimal dynamic treatment regimes. *The International Journal of Biostatistics* 6(2).
- Richardson, T. S. and J. M. Robins (2013). Single world intervention graphs (SWIGs): A unification of the counterfactual and graphical approaches to causality. Technical Report 128, Center for Statistics and the Social Sciences, University of Washington.
- Robins, J. M. (1986). A new approach to causal inference in mortality studies with a sustained exposure period—application to control of the healthy worker survival effect. *Mathematical Modelling* 7, 1393–1512.
- Robins, J. M. (1994). Correcting for non-compliance in randomized trials using structural nested mean models. *Communications in Statistics – Theory and Methods* 23(8), 2379–2412.

- Robins, J. M. (2000). Marginal structural models versus structural nested models as tools for causal inference. In M. E. Halloran and D. Berry (Eds.), *Statistical Models in Epidemiology, the Environment, and Clinical Trials*, pp. 95–133. Springer.
- Robins, J. M. and M. A. Hernán (2009). Estimation of the causal effects of time-varying exposures. In G. Fitzmaurice, M. Davidian, G. Verbeke, and G. Molenberghs (Eds.), *Longitudinal Data Analysis*, pp. 553–599. Boca Raton: CRC Press.
- Robins, J. M., M. A. Hernán, and B. Brumback (2000). Marginal structural models and causal inference in epidemiology. *Epidemiology* 11(5), 550–560.
- Rosenbaum, P. R. (2002). *Observational Studies*. Springer.
- Rubin, D. B. (2004). *Multiple Imputation for Nonresponse in Surveys*, Volume 81. John Wiley & Sons.
- Rubin, D. B. (2005). Causal inference using potential outcomes. *Journal of the American Statistical Association* 100(469), 322–331.
- Siegel, A., B. Cotti-Rausch, D. I. Greenfield, and J. L. Pinckney (2011). Nutrient controls of planktonic cyanobacteria biomass in coastal stormwater detention ponds. *Marine Ecology Progress Series* 434, 15–27.
- Sofrygin, O., M. J. van der Laan, and R. Neugebauer (2016). *simcausal: Simulating Longitudinal Data with Causal Inference Applications*. R package version 0.5.1.99.
- Stefanski, L. A. and D. D. Boos (2002). The calculus of M-estimation. *The American Statistician* 56(1), 29–38.

- Suter, II, G. W., S. B. Norton, and S. M. Cormier (2002). A methodology for inferring the causes of observed impairments in aquatic ecosystems. *Environmental Toxicology and Chemistry* 21(6), 1101–1111.
- U.S. EPA (2015). A compilation of cost data associated with the impacts and control of nutrient pollution. Technical report, U.S. Environmental Protection Agency.
- Vansteelandt, S. and M. Joffe (2014). Structural nested models and g-estimation: The partially realized promise. *Statistical Science* 29(4), 707–731.
- Verbitsky-Savitz, N. and S. W. Raudenbush (2012). Causal inference under interference in spatial settings: A case study evaluating community policing program in Chicago. *Epidemiologic Methods* 1(1), 107–130.
- Wang, Y., M. L. Petersen, D. Bangsberg, and M. J. van der Laan (2006). Diagnosing bias in the inverse probability of treatment weighted estimator resulting from violation of experimental treatment assignment. Technical Report Working Paper 211, U.C. Berkeley Division of Biostatistics Working Paper Series.
- Westreich, D., S. R. Cole, J. G. Young, F. Palella, P. C. Tien, L. Kingsley, S. J. Gange, and M. A. Hernán (2012). The parametric g-formula to estimate the effect of highly active antiretroviral therapy on incident AIDS or death. *Statistics in Medicine* 31(18), 2000–2009.
- Yuan, L. (2010). Estimating the effects of excess nutrients on stream invertebrates from observational data. *Ecological Applications* 20(1), 110–125.
- Yuan, L., A. I. Pollard, S. Pather, J. L. Oliver, and L. D’Anglada (2014). Managing

microcystin: Identifying national-scale thresholds for total nitrogen and chlorophyll *a*.
Freshwater Biology 59(9), 1970–1981.

Supplementary Material for

Upstream Causes of Downstream Effects

A Parametric g-formula formulation

In all of the analyses, the outcome model was parameterized within the g-formula as a linear model:

$$E [Y_{3t} | \bar{A}_t = [0_{t-1} : a_t], \bar{O}_t = \bar{o}_t] = h(\bar{A}, \bar{O}, \beta) \quad (\text{G1})$$

For example, the correctly specified h for the simulations is

$$\beta_0^g + \beta_1^g a_{2t} + \beta_2^g a_{1t} + \beta_3^g l_{12t} + \beta_4^g l_{22t} + \beta_5^g y_{3,t-1}.$$

The stability analyses varied which L covariates were included in h , but the parameterization of the exposure (a_{2t} and a_{1t}) was not modified.

The average potential outcome $E [Y_{3t}([0_{t-1} : a_t])]$ can be linked to observed data in the following manner:

$$\begin{aligned} & E [Y_{3t}([0_{t-1} : a_t])] && (\text{G2}) \\ & = E \{ E [Y_{3t}([0_{t-1} : a_t]) | \bar{A}_{2t} = [0_{t-1} : a_t], \bar{L}_t = \bar{l}_t] \} \quad (\text{no unmeasured confounders}) \\ & = E \{ E [Y_{3t} | \bar{A}_t = [0_{t-1} : a_t], \bar{L}_t = \bar{l}_t] \} \quad (\text{causal consistency}) \end{aligned}$$

According to the parametric g-formula, models for each $f_{l_{pjk}} = f_{l_{pjk}|\bar{l}_{j-1,k-1},\bar{a}_{j-1,k-1}}$ must be fit. However, as will be clear below, the parameters corresponding to non-space- or time-varying covariates cancel in a causal contrast. Hence, we need only fit a model for the conditional mean of L_{22t} , for which we used a standard linear model with expectation $\gamma_0^g + \gamma_1^g l_{12t} + \gamma_2^g l_{22,t-1} + \gamma_3^g a_{1t}$. By causal consistency, $E[L_{22t}(a_{1t})] = \gamma_0^g + \gamma_1^g l_{12t} + \gamma_2^g l_{22,t-1} + \gamma_3^g a_{1t}$. Under this assumed parameterization, $E[L_{22t}(a_{1t}) - L_{22t}(0)] = \gamma_3^g$.

Putting (G2) together with the model for $f_{l_{22t}}$ obtains:

$$\begin{aligned}
& E[Y_{3t}(0_{t-1} : a_t) - Y_{3t}(0_t)] \\
&= E \left\{ E[Y_{3t}(0_{t-1} : a_t) - Y_{3t}(0_t)] \left| A_{1t} = 0, A_{2t} = 0_{t-1} : a_t, \bar{L}_{2t} \right. \right\} \\
&= E \{ \beta_1^g a_{2t} + \beta_2^g a_{1t} + \beta_4^g [L_{22t}(a_{1t}) - L_{22t}(0)] \} \text{ (plugging in } h) \\
&= \beta_1^g a_{2t} + \beta_2^g a_{1t} + \beta_4^g E \{ E[L_{22t}(a_{1t}) - L_{22t}(0) | A_{11} = a_{11}, L_{12t}, L_{22,t-1}] \} \\
&= \beta_1^g a_{2t} + \beta_2^g a_{1t} + \beta_4^g \gamma_3^g.
\end{aligned}$$

When $a_t = (1, 1)'$ for all t , $\mu^g = \frac{1}{n_t} \sum_{t=1}^{n_t} E[Y_{3t}([0_{t-1}, a_t]) - Y_{3t}(0_t)] = \frac{1}{n_t} \sum_{t=1}^{n_t} [\beta_1^g + \beta_2^g + \beta_4^g \gamma_3^g]$.

B Closed form estimator for SNM parameters

Vansteelandt and Joffe (2014) show that a consistent estimator of β^s can found by solving estimating equations (eq. 33):

$$\sum_i \sum_t \sum_s \{ d_{st}(\bar{L}_{ist}, \bar{A}_{ist}) - E[d_{st}(\bar{L}_{ist}, \bar{A}_{ist}) | \bar{L}_{ist}, \bar{A}_{i,s-1,t-1}] \} \{ U_{ist}(\beta^s) - E[U_{ist}(\beta^s) | \bar{L}_{ist}, \bar{A}_{i,s-1,t-1}] \}$$

where $d_{st}(\bar{L}_{ist}, \bar{A}_{ist})$ is chosen to be $E[\partial U_{st}(\beta^s)/\partial \beta^s | \bar{L}_{ist}, \bar{A}_{ist}]$. This formulation is slightly different from Vansteelandt and Joffe in that we added an additional dimension s . Since our endogenous covariate is space-varying rather than time-varying, the blip process is indexed by s rather than t .

Let $\rho_{ist} = E[d_{st}(\bar{L}_{ist}, \bar{A}_{ist}) | \bar{L}_{ist}, \bar{A}_{i,s-1,t-1}]$ and $\lambda_{ist} = E[U_{ist}(\beta^s) | \bar{L}_{ist}, \bar{A}_{i,s-1,t-1}]$, then:

$$\begin{aligned}
& \sum_i \sum_t \{ [d_{1t}(\bar{L}_{i1t}, \bar{A}_{i1t}) - \rho_{i1t}] (U_{i1t}(\beta^s) - \lambda_{i1t}) + [d_{2t}(\bar{L}_{i2t}, \bar{A}_{i2t}) - \rho_{i2t}] (U_{i2t}(\beta^s) - \lambda_{i2t}) \} \\
&= \sum_i \sum_t \left\{ \left[\begin{pmatrix} A_{i2t} \\ 0 \end{pmatrix} - \rho_{i2t} \right] (U_{i1t}(\beta^s) - \lambda_{i1t}) + \left[\begin{pmatrix} A_{i2t} \\ A_{i2t} \end{pmatrix} - \rho_{i2t} \right] (U_{i2t}(\beta^s) - \lambda_{i2t}) \right\} \\
&= \sum_i \sum_t \left\{ \left[\begin{pmatrix} A_{i2t} \\ 0 \end{pmatrix} - \rho_{i2t} \right] (Y_{i3t} - \beta_1^s A_{i2t} - \lambda_{i1t}) \right. \\
&\quad \left. + \left[\begin{pmatrix} A_{i2t} \\ A_{i2t} \end{pmatrix} - \rho_{i2t} \right] (Y_{i3t} - \beta_1^s A_{i2t} - \beta_2^s A_{i1t} - \lambda_{i2t}) \right\} \\
&= \sum_i \sum_t \left\{ \begin{pmatrix} B_{i2t}^0 (r_{i3t} - \beta_1^s A_{i2t}) + B_{i2t}^1 (r_i^0 - \beta_1^s A_{i2t} - \beta_2^s A_{i1t}) \\ B_{i1t}^1 (r_i^1 - \beta_1^s A_{i2t} - \beta_2^s A_{i1t}) \end{pmatrix} \right\}.
\end{aligned}$$

In the last line, we let $B_{ist} = A_{i2t} - \rho_{ist}^k$. Let $r_{ist} = Y_{i3t} - \lambda_{ist}^k$.

Let $C_i = \sum_t r_i^0 (B_{i2t}^0 + B_{i2t}^1)$, $D_i = \sum_t (B_{i2t}^0 A_{i2t} + B_{i2t}^1 A_{i1t})$, $E_i = \sum_t B_{i2t}^1 A_{i1t}$, $F_i = \sum_t B_{i1t}^1 r_i^1$, $G_i = B_{i1t}^1 A_{i2t}$, and $H_i = \sum_t B_{i1t}^1 A_{i1t}$. Then β^s is the solution to:

$$\sum_i \begin{pmatrix} C_i - \beta_1^s D_i - \beta_2^s E_i \\ F_i - \beta_1^s G_i - \beta_2^s H_i \end{pmatrix}$$

which yields,

$$\hat{\beta}_1^s = \frac{\sum_i E_i \sum_i F_i - \sum_i C_i \sum_i H_i}{\sum_i E_i \sum_i G_i - \sum_i D_i \sum_i H_i} \text{ and } \hat{\beta}_2^s = \frac{\sum_i D_i \sum_i F_i - \sum_i C_i \sum_i G_i}{\sum_i D_i \sum_i H_i - \sum_i E_i \sum_i G_i}$$

where

$$\sum_i E_i \sum_i G_i \neq \sum_i D_i \sum_i H_i, \quad \sum_i E_i \neq 0.$$

C Simulation details

The nodes in the simulated study system were parameterized and generated according to the following distributions:

$$\begin{cases}
 t = 0 \left\{ \begin{array}{l}
 L_{110} \sim N(21.5, 2.5) \\
 L_{220} \sim N(-2.8, 0.7) \\
 A_{s0} \sim \text{Bern}(0.1) \text{ for } s = 1, 2 \\
 Y_{30} \sim N(2.25, 1.25)
 \end{array} \right. \\
 t = 1, 2, 3 \left\{ \begin{array}{l}
 L_{11t} \sim N(23 + 0.2L_{11,t-1}, 2) \\
 A_{1t} \sim \text{Bern}(\text{logit}^{-1}(-2.5 + 0.09L_{11t} + 0.025A_{1,t-1})) \\
 L_{12t} \sim N(6.75 + 0.75L_{11,t-1}, 1) \\
 L_{22t} \sim N(2 - 0.04L_{12t} + 0.04L_{22,t-1} + 0.3A_{1t}, 0.25) \\
 A_{2t} \sim \text{Bern}(\text{logit}^{-1}(-2.5 + 0.09L_{12t} + 0.1L_{22t} + 0.05A_{1t} + 0.025A_{2,t-1})) \\
 Y_{3t} \sim N(-5 + 1A_{s-1,t} + 0.5A_{s-2,t} + 0.025L_{1,s-1,t} + 0.5L_{2,s-1,t} + 0.35Y_{3,t-1}, 1)
 \end{array} \right.
 \end{cases}$$

Code for the simulations can be found in the updown R package of the Supplementary Materials.

D Stability analyses

In addition to estimating the target parameters using all possible combinations of settings of the cutpoint and space-varying confounding variables, we also modified the exposure and outcome models to include a temperature by flow interaction term in both outcome and exposure models. This resulted in a total of 1200 point estimates per method. If some component model failed to converge for a method, then the estimate attempt was considered a failure. Across all 3600 attempts, model fitting failed 272 times for the MSMs, 70 times for the SNMs, and zero times for the g-formula.

To check the stability for the primary results presented in Figure 5 to the simple imputation procedure described in the main text, a multiple imputation procedure was used. The `aregImpmute` function from the `Hmisc` R package (Harrell et al., 2017) was used to impute missing values using year, month, distance between sites, flow, temperature, pH, dissolved oxygen, and each of the NP species. Five complete datasets were generated using the predictive mean matching imputation method with the `match='closest'` option. Point estimates from the complete datasets were averaged and the corresponding estimated standard errors pooled using Rubin's rules (Rubin, 2004).

Figure 6 shows all the point estimates within $(-6, 6)$ across all the model options. In two cases, estimates from an SNM were outside this range. The results in Figure 6 conform to the general patterns described in the main text. Figure 7 show all the point estimates along with the p-values using different test statistic distributions. In each panel, the point estimates are the same, but the significance clearly depends on the test statistic

distribution. Figure 8 repeats Figure 5 from the main text using estimates based on the imputation procedure described above.

Figure 6: This figure shows the 3258 point estimates obtained across settings of the cut-point, space-varying confounding variables, and exposure and outcome models. Point estimates for NO_3 between 86 and 109 km upstream are positive across all settings and have the most consistently strong effects. TKN estimates for the two locations just upstream of LD1 are all positive, while the P estimates from the same locations are all negative.

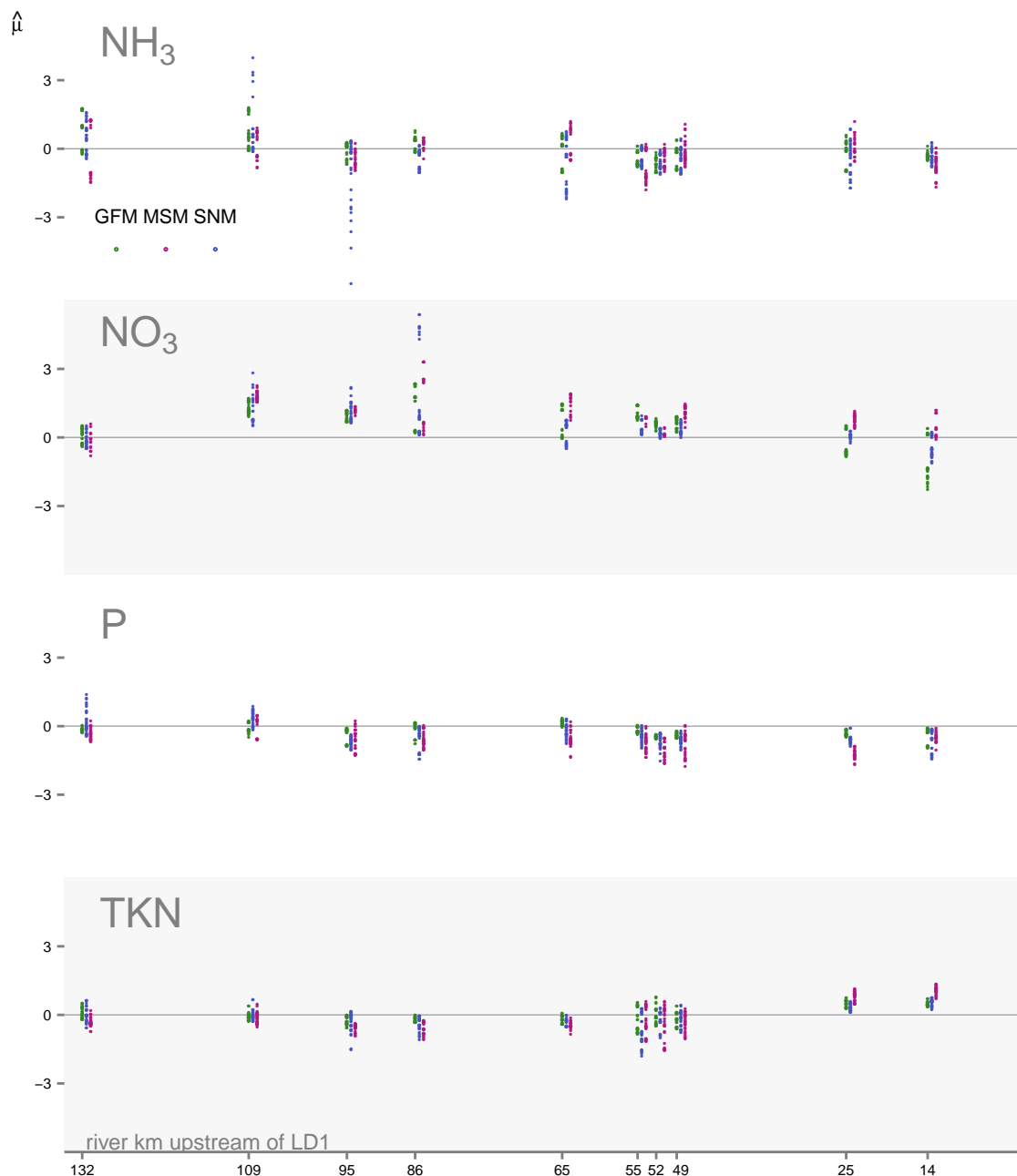


Figure 7: Volcano plot of estimates of the Cape Fear analysis showing significance and estimates for all analysis methods and models. The point estimates are same in all the panels. Significance levels vary depending on the distribution used for the test statistic.

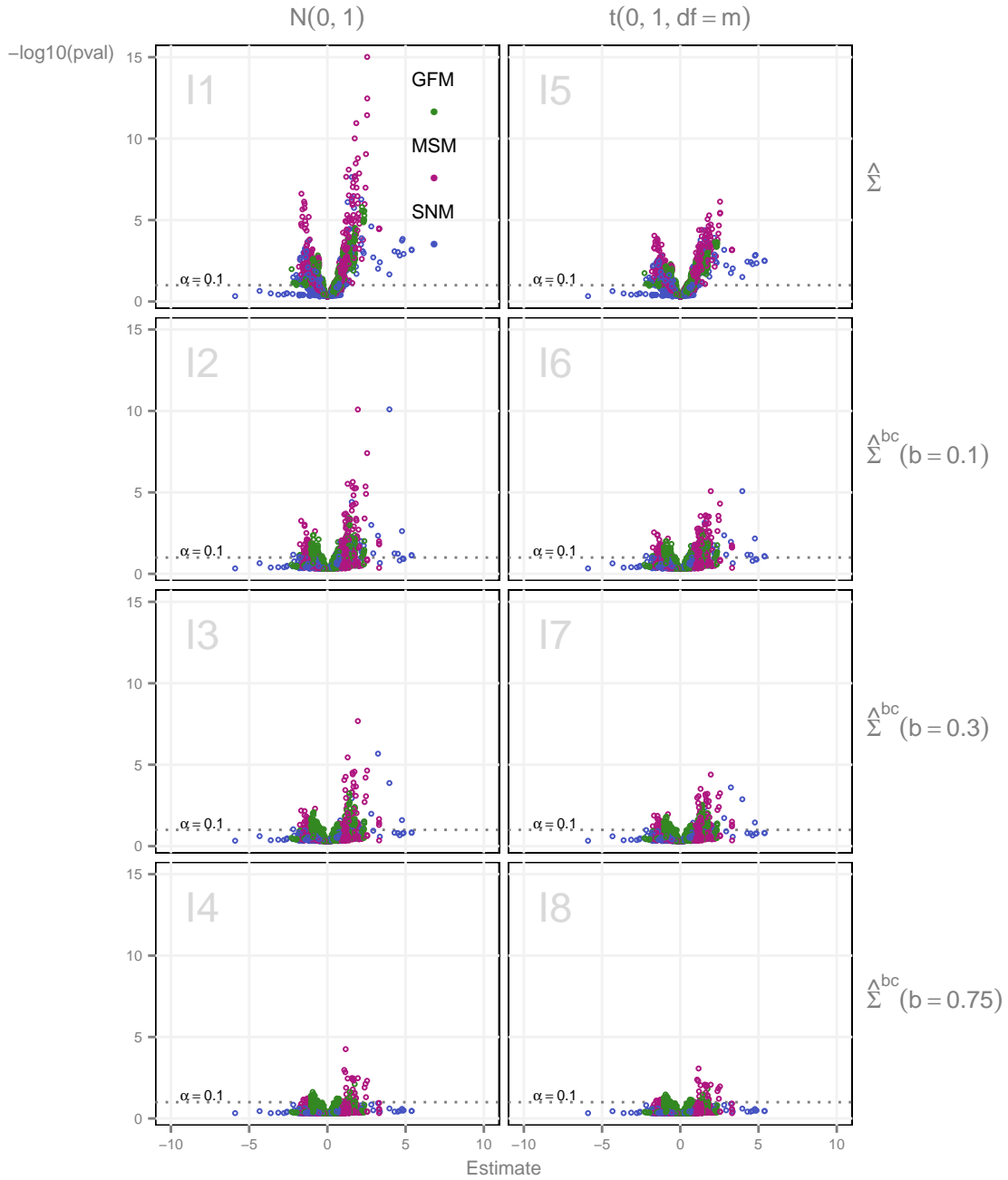


Figure 8: This figure repeats main text Figure 5 with estimates based on the estimated derived from 5 imputed datasets. These results are largely substantively the same as those reported in main text Figure 5.

